applied sciences

MDPI

Article

Similarity Model of a Rotary Lobe Expander Working with Various Fluids

Witold Rybiński *, Artur Maurin, Zbigniew Krzemianowski and Sebastian Bykuć

Institute of Fluid-Flow Machinery, Polish Academy of Sciences, ul. Fiszera 14, 80-231 Gdańsk, Poland; artur.maurin@imp.gda.pl (A.M.); krzemian@imp.gda.pl (Z.K.); sebastian.bykuc@imp.gda.pl (S.B.)
* Correspondence: witold.rybinski@imp.gda.pl

Abstract: This paper presents the similarity model of a rotary lobe expander (Roots expander) and calculates its power based on its other reference power. The rotors in these expanders transfer unchanged gas volume within one rotation. In this model, the expander's construction is represented by the single value of this transferred volume. The derived model concerns the similarity of pressure loss due to the fluid viscosity, which decreases the ideal maximum power of the limiting case of no viscosity. The basic thermodynamic analysis of various fluids is also presented for this case. The novelty is the similarity model of this expander type, which may be used in the analytical and fast engineering calculation of the power before the use of the more precise but expensive numerical calculation. The similarity model is applied to the exemplary rotary lobe expander GGP16XA from Armak Motors. In this paper, the similarity model is applied in two cases. The first application concerns the manufacturer's data on the power from the compressed air of various inlet pressures and rotational speeds. The second one concerns the numerically calculated power from various fluids: Air, R245fa, SES36, and HFE7100, with the power from Air as a reference. The analyzed fluids are used in Organic Rankine Cycle (ORC) applications. In both cases, the obtained similarity power is in good agreement with the reference, with the same maximum relative error ±5%.

Keywords: rotary lobe expander; Roots expander; similarity model; various fluids; Organic Rankine Cycle (ORC)

check for updates

Academic Editor: Nicholas Vassiliou Sarlis

Received: 1 November 2024
Revised: 23 December 2024
Accepted: 24 December 2024
Published: 27 December 2024

Citation: Rybiński, W.; Maurin, A.; Krzemianowski, Z.; Bykuć, S. Similarity Model of a Rotary Lobe Expander Working with Various Fluids. *Appl. Sci.* **2024**, *15*, 120. https://doi.org/10.3390/app15010120

Copyright: © 2024 by the authors. Licensee MDPI, Basel, Switzerland. This article is an open access article distributed under the terms and conditions of the Creative Commons Attribution (CC BY) license (https://creativecommons.org/licenses/by/4.0/).

1. Introduction

There are several types of volumetric expanders. The most popular are the scroll expander [1], screw [2], reciprocating piston [3], rotary vane [4], and rolling piston [5]. In this paper, the rotary lobe expander (Roots expander) is taken into account. This type of expander is special because it has a built-in volume ratio equal to 1, which means that the gas pockets do not change their volume during the rotation [6].

Volumetric expanders are used in many areas. Of special interest is their usage in waste heat recovery and in combined heat and power generation [7,8].

Recently, there have been more publications in which this type of expander is analyzed [6,9,10]. Numerical calculations of the rotary lobe expanders are presented in [11,12]; similar numerical calculations, but for pumps of this type, are presented in [13,14].

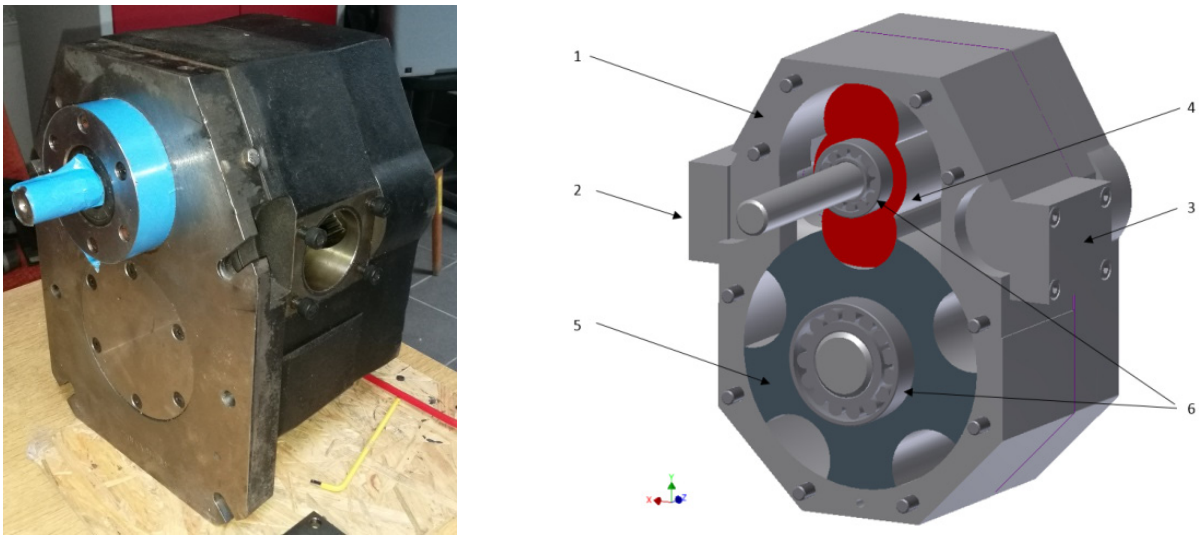
In this paper, the simple analytical model of the power of these expanders is derived. It is based on the similarity theory presented in many books, e.g., in [15,16]. The similarity in the derived models involves the similarity in pressure loss due to fluid viscosity, which decreases the power in case of no viscosity. This similarity allows the usage of known

power from one working fluid in the calculation of the power of another. The construction of the expander is represented by one value of the volume transferred by the rotors during one shaft's revolution. The presented model allows easy calculation of the power for various fluids or for the other working conditions (pressure, rotational speed) before using the more precise but expensive numerical calculation. The authors did not find any studies on existing similarity models for the analyzed rotary lobe expander.

The similarity model was tested on the exemplary rotary lobe expander, the GGP16XA from Armak Motors (Hull, East Yorkshire, UK) [17], due to its higher allowed temperature compared with XGA16. This expander was disassembled and measured.

2. Geometry of the Analyzed Exemplary Rotary Lobe Expander

The analyzed exemplary expander GGP16XA [17] (Figure 1) is originally designed to work with compressed air of the max inlet pressure of 16 bar(a) and the atmospheric outlet one of 1 bar(a), and the max inlet temperature of 150 °C for continuous work. The power is higher than 30 kW for the inlet pressure p_{in} = 16 bar(a) and the rotational speed n = 3000 rpm. The maximum rotational speed is 3500 rpm, with the recommended minimum being 1000 rpm.



(**a**) (**b**)

Figure 1. (**a**) Partially disassembled rotary lobe expander GGP16XA.(**b**) Three-dimensional view of the measured construction: 1 outer casing, 2 outlet, 3 inlet, 4 upper rotor, 5 lower rotor, 6 bearings.

The expander consists of the ø126 mm upper rotor on the expander's shaft and the ø180 mm lower rotor, rotating with 2/5 of the upper rotor's speed. The distance between the rotors' axes is 126 mm. The rotors are 100 mm long and are connected by the gear train. The outer expander's dimensions are 319 × 262 × 265 mm, and the weight is 82 kg.

In the derived similarity model, the construction of the rotary lobe expanders is represented by the volume ΔV_{geom}, transferred by the rotors during one shaft's revolution.

Analysis of the particular rotors' geometry is presented in Appendix A. The volumes transferred in one shaft's revolution by the upper and the lower rotors are analytically derived in Appendix A: $\Delta V_{geom,u} = 5.3718 \cdot 10^{-4}$ m^3 and $\Delta V_{geom,l} = 2.4609 \cdot 10^{-4}$ m^3. The total volume transferred in one shaft's revolution is their sum: $\Delta V_{geom} = 7.8327 \cdot 10^{-4}$ m^3.

The measurement tolerance is ±0.1 mm. For the measurements increased by 0.1 mm, the obtained ΔV_{geom} is $7.8582 \cdot 10^{-4}$ m^3. For the measurements decreased by 0.1 mm, the obtained ΔV_{geom} is $7.8074 \cdot 10^{-4}$ m^3. The relative changes ΔV_{geom} are +0.33% and −0.32%, respectively.

The program in Object Pascal, Delphi 7 Environment, was developed to simulate the expander's geometry at various rotation angles. Figure 2 shows the screenshots from this simulation program. The high-pressure inlet chamber and the low-pressure outlet chamber are in red and blue. The upper and lower high-pressure gas pockets are in magenta and yellow. The rapid gas expansion to the outlet (Figure 2c) does not produce work.

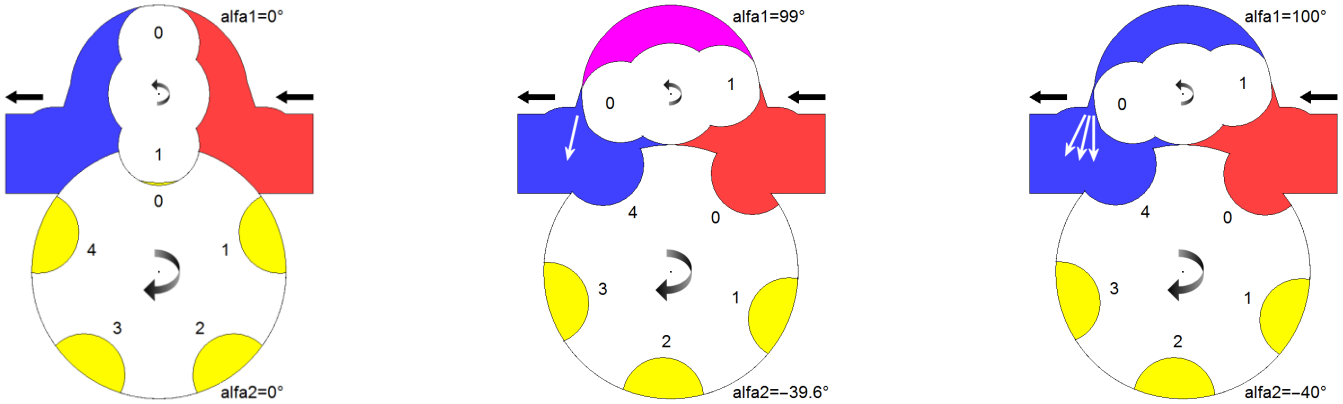


Figure 2. Screenshots from the geometry simulation program. The expander's cross-section (**a**) at an angle of 0, (**b**) just before the opening of the upper high-pressure gas pocket, and (**c**) just after its opening, with no work from this gas expansion (white arrows).

3. Limiting Case of No-Viscosity Fluid

The limiting case of no-viscosity fluid of the expander's power P_0 is the basis for the further-derived similarity model of the actual power P for the real viscous fluids.

The inlet/outlet pressure difference $\Delta p_{in,out}$ is defined as follows:

$$\Delta p_{in,out} = p_{in} - p_{out} \tag{1}$$

In the limiting case of no viscosity, the pressure difference $\Delta p_{,0}$ acting on the rotors is the highest and is equal to $\Delta p_{in,out}$ because there is no pressure loss:

$$\Delta p_0 = \Delta p_{in,out} \tag{2}$$

The limiting and maximum work W_0 produced by the rotors in one shaft's revolution is given as follows:

$$W_0 = \Delta V_{geom} \cdot \Delta p_0 = \Delta V_{geom} \cdot \Delta p_{in,out} \tag{3}$$

where ΔV_{geom} is the volume transferred by the rotors in one shaft's revolution. It is a constant value for the geometry of the particular rotary lobe expander.

It gives the limiting power P_0, applied in the next section of the similarity model:

$$P_0 = n \cdot W_0 = n \cdot \Delta V_{geom} \cdot \Delta p_{in,out} \tag{4}$$

The limiting power P_0 is independent of the fluid because of no viscosity.

The ratio of the upper rotor's power $P_{0,u}$ to the total P_0 is given by the following equation:

$$\frac{P_{0,u}}{P_0} = \frac{n \cdot \Delta V_{geom,u} \cdot \Delta p_{in,out}}{n \cdot \Delta V_{geom} \cdot \Delta p_{in,out}} = \frac{\Delta V_{geom,u}}{\Delta V_{geom}} \tag{5}$$

Substitution of the numerical values (Appendix A) gives $P_{0,u}/P_0 = 0.6858$. The small upper rotor produces 69% of the expander's power P_0 in the limiting case of no viscosity.

The manufacturer's experimental characteristics of the expander's power P_{mnf} for compressed air [17] are compared with the power P_0 of no-viscosity fluid. Figure 3 shows the manufacturer's plot of the power P_{mnf} (solid lines) vs. the rotational speed n, for the inlet air pressure p_{in} = 7...16 bar(a) and the atmospheric outlet one p_{out} = 1 bar(a).

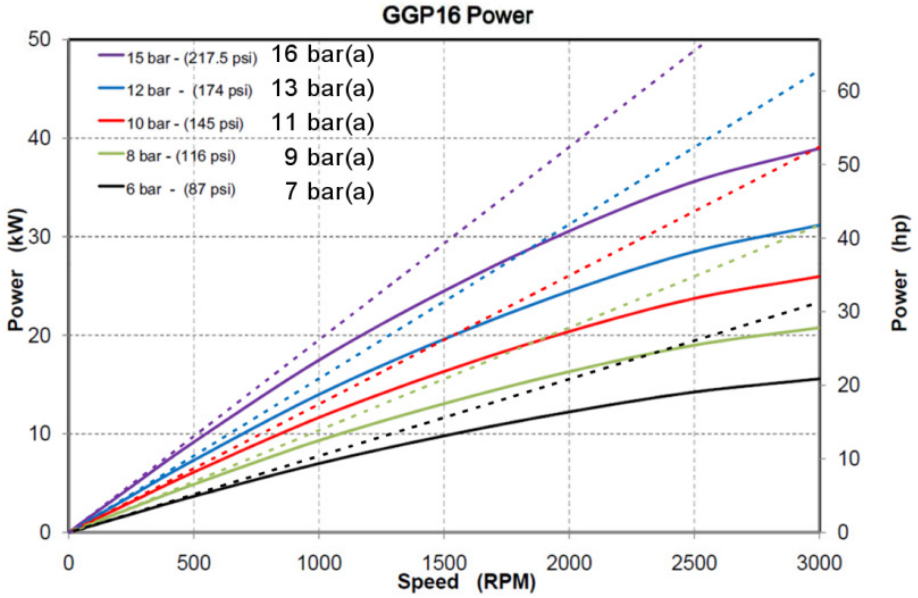


Figure 3. Manufacturer's experimental plot of the expander's power P_{mnf} vs. the rotational speed n, for compressed air [17] (solid lines). The inlet pressure is p_{in} = 7...16 bar(a) and the atmospheric outlet pressure is p_{out} = 1 bar(a). The limiting power P_0 of a no-viscosity fluid (dashed lines) is drawn over the original plot.

The limiting power P_0 (4) of no viscosity (dashed lines) is drawn over the original manufacturer's plot. At the low rotational speed, n, the influence of viscosity is almost negligible, and the actual experimental power P_{mnf} is close to the limiting power P_0.

The expander's power P depends on the mass flow rate and the specific enthalpy change:

$$P = \dot{m} \cdot \Delta h = \dot{m} \cdot [h(p_{in}, T_{in}) - h(p_{out}, T_{out})] \quad (6)$$

where the mass flow rate is given by the inlet volumetric flow rate $\dot{V}_{in}$:

$$\dot{m} = \rho_{in} \cdot \dot{V}_{in} \quad (7)$$

In the case of no viscosity, the inlet volumetric flow rate $\dot{V}_{in,0}$ is equal to the volumetric rate $\dot{V}_{geom}$ taken and transferred by the rotors, $\dot{V}_{in,0} = \dot{V}_{geom}$ because there is no pressure loss or density change from the inlet to the rotors.

For the real viscous fluids, the inlet pressure p_{in} and the density ρ_{in} are higher than those near the rotors, which means the volumetric flow rates $\dot{V}_{in} < \dot{V}_{geom}$.

The geometric flow rate transferred by the rotors is given by the following equation:

$$\dot{V}_{geom} = n \cdot \Delta V_{geom} \quad (8)$$

The mass flow rate taken by the rotors in the case of no viscosity is given by the following equation:

$$\dot{m}_0 = \rho_{in} \cdot \dot{V}_{in,0} = \rho_{in} \cdot \dot{V}_{geom} \quad (9)$$

In this case, the limiting power P_0 is given by the following equation:

$$P_0 = \dot{m}_0 \cdot \Delta h_0 = \rho_{in} \cdot \dot{V}_{geom} \cdot \Delta h_0 \quad (10)$$

where Δh_0 is the specific enthalpy change in the case of no viscosity.

The combination of (4), (7), and (10) gives the formula for the specific enthalpy change Δh_0 in the case of no viscosity, independent of the rotational speed n:

$$\Delta h_0 = \frac{\Delta p_{in,out}}{\rho_{in}} \quad (11)$$

The value of Δh_0 (11) allows calculation of the corresponding outlet temperature $T_{out,0}$, by solving the equation for $T_{out,0}$:

$$h(p_{in}, T_{in}) - h(p_{out}, T_{out,0}) = \Delta h_0 \quad (12)$$

The corresponding outlet density $\rho_{out,0}$ is given by the following equation:

$$\rho_{out,0} = \rho(p_{out}, T_{out,0}) \quad (13)$$

The highest available power P_s from the isentropic expansion between the inlet and outlet, for the same mass flow rate $\dot{m}_0$ as in (10) and the same inlet and outlet pressures, is given by the following equation:

$$P_s = \dot{m}_0 \cdot \Delta h_s \quad (14)$$

where the isentropic change in the specific enthalpy Δh_s is given by the following equation:

$$\Delta h_s = h(p_{in}, T_{in}) - h(p_{out}, s_{in}) \quad (15)$$

with the inlet-specific entropy:

$$s_{in} = s(p_{in}, T_{in}) \quad (16)$$

A combination of (10) and (14) gives the isentropic efficiency $\eta_{s,0}$ for the limiting case of no viscosity, independent of the rotational speed n:

$$\eta_{s,0} = \frac{P_0}{P_s} = \frac{\Delta h_0}{\Delta h_s} \quad (17)$$

In Table 1, the calculation results for the limiting case of no viscosity are presented for the expander working with compressed air and with the other fluids R245fa, SES36, and HFE7100 in the Organic Rankine Cycle (ORC).

Table 1. Limiting case of no viscosity for the expander working with compressed air and with the other fluids in the ORC. P_0, P_s, and m_0 are calculated for the rotational speed n = 3000 rpm.

Fluid	p_{in} Bar(a)	T_{in} °C	ρ_{in} kg/m^3	p_{out} Bar(a)	$T_{out,0}$ °C	$\rho_{out,0}$ kg/m^3	P_0 kW	P_s kW	$\eta_{s,0}$ %	m_0 kg/s
Air	16.0	25.0	18.78	1.0	−57.8	1.62	58.7	119.1	49.3	0.736
R245fa	16.0	115.8	91.09	1.0	74.1	4.74	58.7	187.3	31.4	3.567
SES36	16.0	149.8	125.9	1.0	94.1	6.22	58.7	192.8	30.5	4.931
HFE7100	16.0	179.6	175.9	1.0	153.8	7.21	58.7	233.5	25.2	6.889

The inlet pressure is p_{in} = 16 bar(a), the atmospheric outlet pressure is p_{out} = 1 bar(a) and the rotational speed is n = 3000 rpm. In the ORC, the inlet temperature T_{in} is 5 °C higher than the boiling temperature of the working fluid at the inlet pressure p_{in}.

Each no-viscosity power P_0 (4) is the same as it depends only on the pressure difference $\Delta p_{in,out}$ and the rotational speed n. The isentropic power P_s (14) depends on the fluid, which makes the values of the isentropic efficiency $\eta_{s,0}$ (17) different.

Even in the ideal case of no viscosity, the isentropic efficiency $\eta_{s,0}$ is far below 100% due to the expander's principle of operation with an unproductive gas expansion to the outlet, which strongly decreases the power. The rapid expansion of the gas to the outlet is a real viscous dissipation process of mechanical energy.

The intention of this basic thermodynamic analysis is to show the thermodynamic differences among the working fluids without viscosity effects being taken into account.

Figure 4 shows the isentropic efficiency $\eta_{s,0}$ vs the inlet pressure p_{in} for the analyzed fluids. The efficiency $\eta_{s,0}$ increases to 100% as the inlet pressure p_{in} reduces to the outlet pressure p_{out}, while the expander's power reduces to 0.

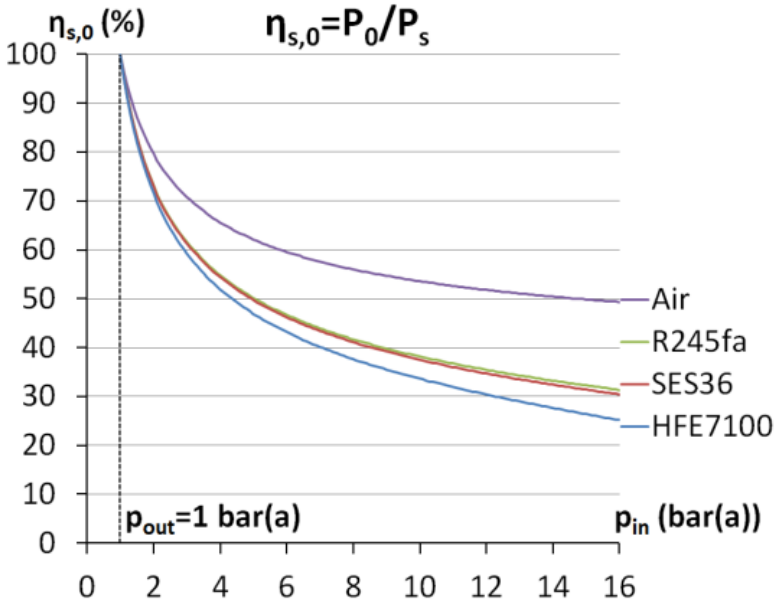


Figure 4. Isentropic efficiency $\eta_{s,0}$ vs. the inlet pressure p_{in} in the ideal case of no viscosity for compressed air and for the other fluids working in the ORC.

The limiting power P_0 (4) and the specific enthalpy change Δh_0 (11) are also analyzed regarding sensitivity to the variations in the quantities in these equations. The uncertainties in P_0 and Δh_0 are determined by the use of the propagation of uncertainty [18,19].

The relative uncertainty of P_0, for uncorrelated n, ΔV_{geom}, $\Delta p_{in,out}$ in (4), is given by the following equation:

$$\left(\frac{S_{P_0}}{P_0}\right)^2 = \left(\frac{S_n}{n}\right)^2 + \left(\frac{S_{\Delta V_{geom}}}{\Delta V_{geom}}\right)^2 + \left(\frac{S_{\Delta p_{in,out}}}{\Delta p_{in,out}}\right)^2 \quad (18)$$

The relative uncertainty of ΔV_{geom} is determined in Section 2. $S_{\Delta Vgeom}/\Delta V_{geom}$ = 0.33%. The remaining relative uncertainties are assumed as S_n/n = 5%, $S_{\Delta pin,out}/\Delta p_{in,out}$ = 5%. The obtained relative uncertainty is S_{P0}/P_0 = 7.08%.

The specific enthalpy change Δh_0 (11) may be directly compared with the same quantity of the real, viscous working fluid. The relative uncertainty of Δh_0, for uncorrelated $\Delta p_{in,out}$, ρ_{in} in (11), is given by the following equation:

$$\left(\frac{S_{\Delta h_0}}{\Delta h_0}\right)^2 = \left(\frac{S_{\Delta p_{in,out}}}{\Delta p_{in,out}}\right)^2 + \left(\frac{S_{\rho_{in}}}{\rho_{in}}\right)^2 \tag{19}$$

The relative uncertainties are assumed as $S_{\Delta pin,out}/\Delta p_{in,out} = 5\%$, $S_{\rho in}/\rho_{in} = 5\%$. The obtained relative uncertainty is $S_{\Delta h0}/\Delta h_0 = 7.07\%$.

4. Similarity Model for Viscous Working Fluids

The presented limiting power P_0 (4) of no viscosity is the basis for the similarity model of the actual expander's power P working with viscous fluids.

The derived model concerns the similarity of the pressure loss Δp_{loss} due to the fluid's viscosity, which decreases the expander's power.

The actual power P is less than the limiting power P_0 due to the pressure loss Δp_{loss}, mainly because of the fluid viscosity. The influence of internal leakage is not analyzed in this paper for the rotational speed n above the recommended minimum of 1000 rpm.

The actual pressure difference Δp acting on the rotors is less than the inlet/outlet pressure difference $\Delta p_{in,out}$ by the total pressure loss Δp_{loss}:

$$\Delta p = \Delta p_{in,out} - \Delta p_{loss} \tag{20}$$

Both Δp and Δp_{loss} are mean values within one shaft's rotation.

The actual expander's power P is a modification of the limiting power P_0 (4), where $\Delta p_{in,out}$ is replaced by Δp (20), which makes the actual power $P < P_0$:

$$P = n \cdot \Delta V_{geom} \cdot \Delta p = n \cdot \Delta V_{geom} \cdot \left(\Delta p_{in,out} - \Delta p_{loss}\right) \tag{21}$$

In the presented similarity model, the pressure losses are not separated and are represented by the single total pressure loss Δp_{loss} between the inlet and the equivalent piston (Figure 5). Both rotors with a constant rotational speed are represented by the single piston with a constant velocity, jumping back to the beginning in every cycle. This way, in this model, the fluid flow and the pressure loss are constant between the inlet and the equivalent piston.

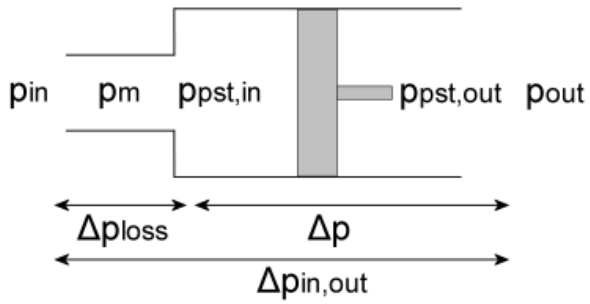


Figure 5. The model of the single inlet pressure loss Δp_{loss} representing the total pressure losses.

Although the assumption of the single, constant pressure loss Δp_{loss} may seem rather coarse, the results of the derived similarity model are in good agreement with the manufacturer's experimental data and with the results of the numerical calculation.

In this simplified model, the pressure $p_{pst,in}$ near the piston is given by the following equation:

$$p_{pst,in} = p_{in} - \Delta p_{loss} \tag{22}$$

Pressure drop Δp_{loss} in the incompressible viscous flow is a well-known phenomenon [20] and is represented by the general relationship between the Euler and Reynolds numbers:

$$\mathrm{Eu} = \mathrm{f}(\mathrm{Re}) = A \cdot \left(\frac{1}{\mathrm{Re}}\right)^{\gamma} \tag{23}$$

The coefficient A depends on the channel's geometry and the flow type and is reduced in further derivation. The exponent γ depends on the flow type: $\gamma = 1$ for laminar flows, $\gamma = 0.25$ for turbulent flows (the Blasius formula), and $\gamma = 0$ for local losses (valves, sudden channel contraction/expansion, etc.) or for very turbulent flows. These pure cases cover the range of the possible cases and generally $0 \leq \gamma \leq 1$.

However, for the compressible gas, the pressure drop Δp_{loss} from the inlet to the piston makes the fluid's density change significant. In this case, the simplified concept of the mean gas pressure p_m and the corresponding mean gas density ρ_m [21] is used.

The mean pressure p_m (Figure 5) is assumed to be the arithmetic mean of p_{in} and $p_{pst,in}$:

$$p_m = \left(p_{in} + p_{pst,in}\right)/2 = p_{in} - \Delta p_{loss}/2 \tag{24}$$

The explicit form of the Euler and Reynolds numbers in (23) gives the equation:

$$\frac{\Delta p_{loss}}{\rho_m \cdot v_m^2/2} = A \cdot \left(\frac{\mu_m}{v_m \cdot d_h \cdot \rho_m}\right)^{\gamma} \tag{25}$$

with the mean fluid density ρ_m and viscosity μ_m at the mean pressure p_m, and with the equivalent hydraulic diameter d_h reduced further.

The mean fluid velocity v_m is calculated using the same mass flow rate $\dot{m}$ at the mean pressure p_m and at the pressure $p_{pst,in}$ near the piston, with the known volumetric flow rate $\dot{V}_{geom}$ transferred by the piston:

$$\dot{m} = \rho_m \cdot \dot{V}_m = \rho_{pst,in} \cdot \dot{V}_{geom} \tag{26}$$

It gives the volumetric flow rate $\dot{V}_m$ for the mean density ρ_m:

$$\dot{V}_m = \frac{\rho_{pst,in}}{\rho_m} \cdot \dot{V}_{geom} \tag{27}$$

The mean fluid velocity v_m used in (25) is calculated using the mean channel's cross-sectional area S_m, which is reduced further:

$$v_m = \frac{\dot{V}_m}{S_m} = \frac{\rho_{pst,in}}{\rho_m} \cdot \frac{\dot{V}_{geom}}{S_m} = \frac{\rho_{pst,in}}{\rho_m} \cdot \frac{n \cdot \Delta V_{geom}}{S_m} \tag{28}$$

The combination of (25) and (28) gives the formula for the pressure loss Δp_{loss}:

$$\Delta p_{loss} = \frac{A}{2 \cdot d_h^{\gamma}} \cdot \mu_m^{\gamma} \cdot \rho_m^{1-\gamma} \cdot \left(\frac{\rho_{pst,in}}{\rho_m} \cdot \frac{n \cdot \Delta V_{geom}}{S_m}\right)^{2-\gamma} \tag{29}$$

This formula is converted to the form in which the right-hand side depends only on the geometry of the particular expander:

$$\frac{\Delta p_{loss}}{\mu_m^{\gamma} \cdot \frac{\rho_{pst,in}^{2-\gamma}}{\rho_m} \cdot n^{2-\gamma}} = \frac{A \cdot \Delta V_{geom}^{2-\gamma}}{2 \cdot d_h^{\gamma} \cdot S_m^{2-\gamma}} \tag{30}$$

This way, the left-hand side in (30) also depends only on the geometry of the particular expander.

It gives the similarity equation for the pressure loss Δp_{loss} with the similarity parameter B of the particular expander:

$$\frac{\Delta p_{loss}}{\mu_m^{\gamma} \cdot \frac{\rho_{pst,in}^{2-\gamma}}{\rho_m} \cdot n^{2-\gamma}} = B \tag{31}$$

The flow from the inlet to the piston is an isenthalpic process and is approximated by the isothermal process of the perfect gas. The Clapeyron equation gives the density:

$$\rho = \frac{m}{V} = \frac{p \cdot M_{mol}}{R \cdot T} \tag{32}$$

It gives the gas densities at the inlet pressure p_{in}, at the mean pressure p_m between the inlet and the piston, at the pressure $p_{pst,in}$ near the piston, for the same temperature T_{in}:

$$\rho_{in} = \frac{p_{in} \cdot M_{mol}}{R \cdot T_{in}} \quad \rho_m = \frac{p_m \cdot M_{mol}}{R \cdot T_{in}} \quad \rho_{pst,in} = \frac{p_{pst,in} \cdot M_{mol}}{R \cdot T_{in}} \tag{33}$$

which, using (22) and (24), gives the following:

$$\frac{\rho_m}{\rho_{in}} = 1 - \Delta p_{loss}/(2 \cdot p_{in}) \quad \frac{\rho_{pst,in}}{\rho_{in}} = 1 - \Delta p_{loss}/p_{in} \tag{34}$$

The equations in (34) are substituted into Equation (31), and the viscosity μ_m in (31) is replaced by the known inlet μ_{in} since gas dynamic viscosity weakly depends on the pressure.

The final similarity equation for the pressure loss Δp_{loss}, with the parameter B for the particular expander, is given by the following equation:

$$\frac{\Delta p_{loss}}{\mu_{in}^{\gamma} \cdot \rho_{in}^{1-\gamma} \cdot \frac{(1-\Delta p_{loss}/p_{in})^{2-\gamma}}{1-\Delta p_{loss}/(2 \cdot p_{in})} \cdot n^{2-\gamma}} = B \tag{35}$$

In the next sections, examples used to determine γ and B are presented.

5. Manufacturer's Experimental Data for Power from Compressed Air

Table 2 presents the manufacturer's experimental power P_{mnf} from compressed air, read from the original plot in [17] and also shown in Figure 3 (solid lines).

The inlet pressure is p_{in} = 7...16 bar(a), the atmospheric outlet pressure is p_{out} = 1 bar(a), and the rotational speed is n = 250, 500, . . . 3000 rpm.

To the best of the authors' knowledge, the manufacturer's plot in [17] is probably the only published experimental data for the analyzed expander type. The inlet air temperature is not presented. The lines in this plot are probably smoothed based on the unknown number of measurements.

Table 2. Manufacturer's experimental power P_{mnf} for air [1], also in Figure 3 (solid lines), for p_{in} = 7...16 bar(a) and p_{out} = 1 bar(a).

n rpm	P_{mnf}, kW				
	7 Bar(a)	**9 Bar(a)**	**11 Bar(a)**	**13 Bar(a)**	**16 Bar(a)**
0	0.000	0.000	0.000	0.000	0.000
250	1.830	2.440	3.080	3.720	4.630
500	3.650	4.870	6.090	7.310	9.130
750	5.350	7.140	8.930	10.720	13.430
1000	6.970	9.300	11.670	13.970	17.460
1250	8.420	11.270	14.070	16.880	21.110
1500	9.780	13.020	16.310	19.590	24.490
1750	11.030	14.750	18.400	22.120	27.670
2000	12.210	16.310	20.370	24.460	30.550
2250	13.260	17.730	22.160	26.620	33.250
2500	14.240	18.980	23.710	28.480	35.590
2750	14.920	19.930	24.900	29.910	37.380
3000	15.560	20.770	25.950	31.160	38.940

6. Similarity Analysis of the Manufacturer's Experimental Data for Air

The first application of the similarity model uses the manufacturer's experimental data for air [17] (Table 2).

The measurements of P_{mnf} are in Table 2 for p_{in} = 7...16 bar(a) and p_{out} = 1 bar(a). The assumed inlet temperature is T_{in} = 25 °C, which is not given by the manufacturer. The applied rotational speed is n = 750, 1000...3000 rpm because 1000 rpm is the recommended minimum rotational speed.

The manufacturer's power P_{mnf} is approximated by the similarity power P_{sim} for the corresponding inlet/outlet pressure difference $\Delta p_{in,out}$ and the rotational speed n.

The similarity power P_{sim} is calculated from (21):

$$P_{sim} = n \cdot \Delta V_{geom} \cdot \left(\Delta p_{in,out} - \Delta p_{loss,sim} \right) \tag{36}$$

where the similarity pressure loss $\Delta p_{loss,sim}$ is calculated by numerically solving Equation (35) with the inlet viscosity μ_{in} and density ρ_{in} for the inlet pressure p_{in} and temperature T_{in}:

$$\frac{\Delta p_{loss,sim}}{\mu_{in}^{\gamma} \cdot \rho_{in}^{1-\gamma} \cdot \frac{\left(1-\Delta p_{loss,sim}/p_{in}\right)^{2-\gamma}}{1-\Delta p_{loss,sim}/(2 \cdot p_{in})} \cdot n^{2-\gamma}} = B \tag{37}$$

The parameters γ and B are approximated from the manufacturer's experimental power P_{mnf} via minimization of the function $\phi(\gamma,B)$ (38).

This function is the maximum absolute value of the relative difference between the similarity P_{sim} and the manufacturer's power P_{mnf}. It is determined using the all-inlet pressures p_{in} and rotational speeds n:

$$\varphi(\gamma, B) = Max\left[\left| \left(P_{sim} - P_{mnf} \right) / P_{mnf} \right| : p_{in} = 7...16 bar(a), n = 750...3000 \text{ rpm} \right] \tag{38}$$

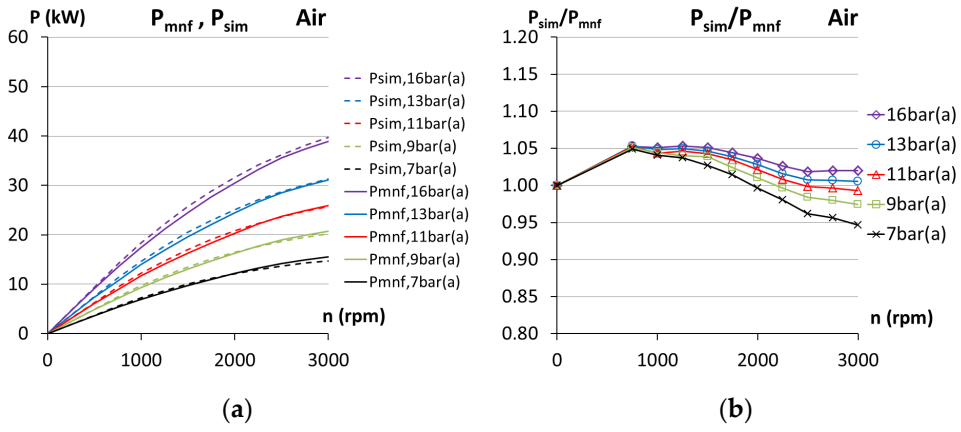
The minimization of $\phi(\gamma,B)$ is the approximation in the maximum norm [22] of P_{mnf} by P_{sim}. It is different from the least squares minimization [22] and it minimizes the maximum relative difference between P_{sim} and P_{mnf}.

The Nelder–Mead method of minimization of $\phi(\gamma,B)$ gives γ = 0.10886 (−) and B = 119.8676, which is not dimensionless. The units of B are complicated; as in (31), they depend on the value of γ.

The similarity power P_{sim} and the ratio P_{sim}/P_{mnf} are presented in Table 3 and Figure 6. The ratio P_{sim}/P_{mnf} is calculated to compare P_{sim} and P_{mnf} and to present the relative errors of the approximation of P_{mnf} by P_{sim}. The maximum relative error of P_{sim} vs. P_{mnf} in the analyzed ranges of the pressure and the rotational speed is about ±5% (Table 3 and Figure 6b). The obtained similarity power P_{sim} is in rather good agreement with the manufacturer's experimental power P_{mnf}.

Table 3. Similarity power for air P_{sim} and the ratio P_{sim}/P_{mnf} of the similarity power and the manufacturer's experimental power for p_{in} = 7...16 bar(a) and p_{out} = 1 bar(a).

n rpm	P_{sim}, kW					P_{sim}/P_{mnf}, –				
	7 Bar(a)	9 Bar(a)	11 Bar(a)	13 Bar(a)	16 Bar(a)	7 Bar(a)	9 Bar(a)	11 Bar(a)	13 Bar(a)	16 Bar(a)
0	0.000	0.000	0.000	0.000	0.000	1.0000	1.0000	1.0000	1.0000	1.0000
250	–	–	–	–	–	–	–	–	–	–
500	–	–	–	–	–	–	–	–	–	–
750	5.612	7.503	9.397	11.291	14.134	1.0490	1.0509	1.0522	1.0532	1.0524
1000	7.252	9.714	12.180	14.649	18.355	1.0404	1.0446	1.0437	1.0486	1.0513
1250	8.731	11.724	14.722	17.724	22.234	1.0370	1.0403	1.0463	1.0500	1.0532
1500	10.043	13.520	17.005	20.498	25.747	1.0269	1.0384	1.0426	1.0463	1.0513
1750	11.186	15.102	19.031	22.969	28.891	1.0141	1.0239	1.0343	1.0384	1.0441
2000	12.168	16.479	20.807	25.147	31.676	0.9966	1.0104	1.0214	1.0281	1.0369
2250	13.000	17.664	22.349	27.049	34.125	0.9804	0.9963	1.0085	1.0161	1.0263
2500	13.695	18.673	23.676	28.699	36.263	0.9617	0.9838	0.9986	1.0077	1.0189
2750	14.268	19.525	24.811	30.120	38.119	0.9563	0.9797	0.9964	1.0070	1.0198
3000	14.732	20.236	25.774	31.338	39.724	0.9468	0.9743	0.9932	1.0057	1.0201



(**a**) (**b**)

Figure 6. (**a**) Comparison of the manufacturer's experimental power P_{mnf} for air [17] (solid lines, also in Figure 3) with the similarity power P_{sim} (dashed lines) vs. the rotational speed n = 750...3000 rpm; (**b**) the ratio P_{sim}/P_{mnf} for the comparison of P_{sim} and P_{mnf}.

7. Numerical Calculation of the Power for Air and the Other Fluids

The numerical Immersed Solid method in the program ANSYS/CFX 19.1 was used to calculate the power P_{num} for Air, R245fa, SES36, and HFE7100 for two rotational speeds: n = 1500 and 3000 rpm.

Figure 7 shows the meshes of the fluid and the solid domain. The thickness of the domains is 10 mm. The results of the numerical calculation are multiplied by 10 to obtain the power P_{num} for 100 mm long rotors.

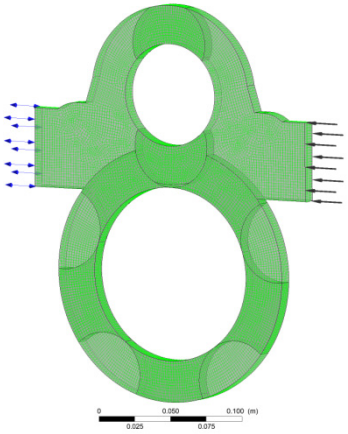


Figure 7. Meshes of the fluid and two solid domains.

The number of used cells and their nodes for the fluid and two solid domains are presented in Table 4.

Table 4. Number of nodes and cells in the domains.

Domain	Number of Nodes	Number of Cells
Total model	293,976	62,088
Fluid	222,053	47,748
Upper rotor	21,236	4305
Lower rotor	50,687	10,035

Clearance among the rotors and the housing is not taken into account. The used turbulence model is two-equation RANS (Reynolds Averaged Navier–Stokes) k-ε (Scalable Wall Function), with turbulence intensity of 5%. The time step is 0.0002 s (3.6° and 1.8° of the upper and lower rotors, respectively, at 3000 rpm of the shaft). In one time step, there are 10 iterations. The discretization is the Second Order Backward Euler. The other settings are advection scheme: high resolution; residual type: root mean square (RMS); and convergence: 10^{-4}.

One of the subsequent stages of calculations of the rotary lobe expander involved performing the mesh independence test. The aim was to examine the influence of grid density on the obtained computational results. In this case, the calculation was conducted for two grid densities. One of them corresponds to the grid whose number of elements is presented in Table 4. In the second case, the aforementioned grid was doubled in density. The results of the comparison between these two types of calculations are shown in Figure 8 using the example of the output power for the given inlet pressure p_{in} = 16 bar(a) of air, outlet pressure p_{out} = 1 bar(a), and rotational speed n = 3000 rpm.

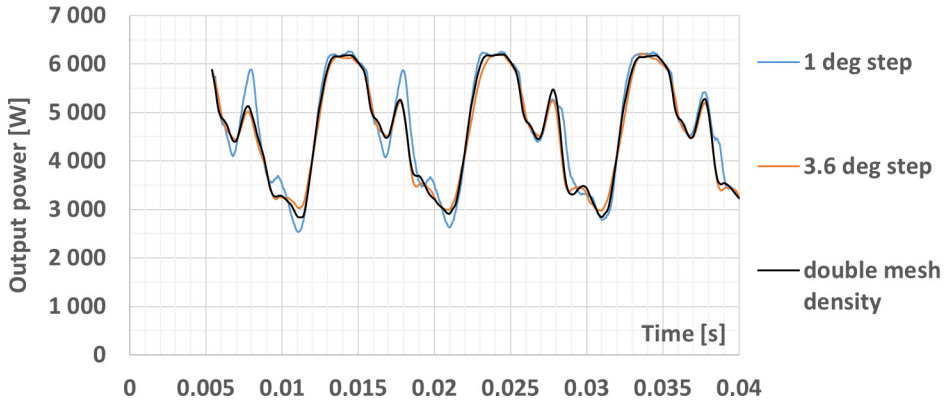


Figure 8. Instantaneous output power as a function of the rotational angle of the upper rotor (the expander's shaft) for the various computational scenarios of the rotational angle and the numerical grid density, given the inlet pressure p_{in} = 16 bar(a) of air, the outlet pressure p_{out} = 1 bar(a), and the rotational speed n = 3000 rpm.

The mesh independence was tested during the first two revolutions of the upper rotor because of the high cost of the calculation. The comparison indicates relatively good consistency in the calculation, as demonstrated in Table 5—the relative difference amounted to approximately 0.53%. For this reason, it was decided to continue the calculation using the coarser grid (Table 4), which, as in the case described above (for the time step), directly contributed to saving computational time and the required disk space.

Table 5. Mean values of the output power P for air depending on the rotational angle of the upper rotor (the expander's shaft) during its two first revolutions for the pressure difference $\Delta p_{in,out}$ = 15 bar and the rotational speed n = 3000 rpm. The upper rotor's increment in the rotational angle is 3.6° (0.0002 s).

p_{in} = 16 Bar(a) p_{out} = 1 Bar(a)	Single Grid Density, Table 4	Double Grid Density	Relative Difference, (%)
Mean output power, kW	45.984	46.229	0.53

The values used in the calculation (Table 6) are the same as in Table 1. Only the air density ρ_{in} is different at the fourth digit because in ANSYS/CFX, it is calculated from the Clapeyron equation. The dynamic viscosity μ_{in} of HFE7100 is calculated using the Licht–Stechert formula.

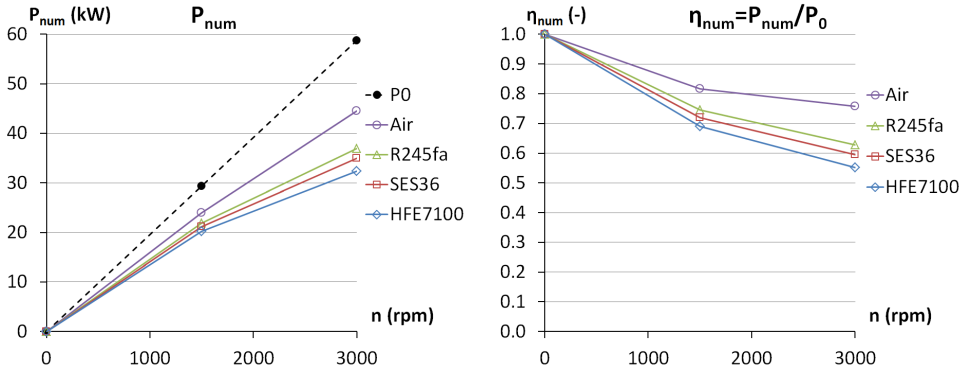
Table 6. Values used in the numerical calculation and the critical parameters of the working fluids.

Fluid	p_{in} Bar(a)	T_{in} °C	ρ_{in} kg/m^3	$\mu_{in}\cdot 10^5$ kg/ms	p_{out} Bar(a)	p_{cr} Bar(a)	T_{cr} °C	ρ_{cr} kg/m^3
Air	16.0	25.0	18.70	1.831	1.0	37.86	−140.6	342.9
R245fa	16.0	115.8	91.09	1.440	1.0	36.51	154.0	516.1
SES36	16.0	149.8	125.9	1.841	1.0	28.49	177.6	517.6
HFE7100	16.0	179.6	175.9	1.553	1.0	22.29	195.3	555.0

The numerical results of the stabilized calculation after the first four revolutions of the upper rotor, the P_{num} and $\eta_{num} = P_{num}/P_0$ are presented in Table 7 and Figure 9.

Table 7. Numerical power P_{num} and efficiency $\eta_{num} = P_{num}/P_0$ for p_{in} = 16 bar(a) and p_{out} = 1 bar(a).

n rpm	P_{num}, kW					$\eta_{num} = P_{num}/P_0$, –			
	HFE7100	**SES36**	**R245fa**	**Air**	P_0	**HFE7100**	**SES36**	**R245fa**	**Air**
0	0.000	0.000	0.000	0.000	0.000	1.0000	1.0000	1.0000	1.0000
1500	20.255	21.142	21.905	24.000	29.373	0.6896	0.7198	0.7458	0.8171
3000	32.379	34.946	36.891	44.550	58.745	0.5512	0.5949	0.6280	0.7584



(**a**) (**b**)

Figure 9. (**a**) Numerical power P_{num} vs. the rotational speed n for various working fluids and (**b**) efficiency $\eta_{\text{num}} = P_{num}/P_0$. The dashed line shows the limiting power P_0 of the no-viscosity fluid.

The same expander type, but with the lower rotor on the expander's shaft, was numerically analyzed for air in [11]. They used the same Immersed Solid method in ANSYS/CFX; however, for the rotational speed of the upper rotor, they used n = 2500 and 3750 rpm.

The open question is the difference between the manufacturer's power $P_{mnf,Air}$ = 38.940 kW and the numerically calculated $P_{num,Air}$ = 44.550 kW for the same n = 3000 rpm, p_{in} = 16 bar(a), and p_{out} = 1 bar(a).

It may be partly caused by the assumed lack of clearance among the rotors and the housing in the calculation and by the possibly different inlet temperatures T_{in} for P_{num} and P_{mnf}, which are not presented in the manufacturer's data.

The main reason seems to be the assumed (forced) outlet pressure p_{out} = 1 bar(a) at the end of the fluid domain, i.e., at the end of the outlet chamber. In reality, the fluid (Air) cannot go out fast enough at the high rotational speed of 3000 rpm to achieve p_{out} = 1 bar(a) in this place. The actual outlet pressure is higher and the actual power is lower.

The same issue is analyzed in [11] for the rotational speed of 3750 rpm for the upper rotor, where the pressure 1 bar(a) at the outlet makes the calculated numerical power too high in comparison with the manufacturer's data. After increasing this pressure to 1.4 bar(a), the authors of [11] obtained good agreement between the calculated power and the manufacturer's power.

For n = 1500 rpm, the values $P_{mnf,Air}$ = 24.490 kW and $P_{num,Air}$ = 24.000 kW are in good agreement.

Because of this discrepancy, the manufacturer's P_{mnf} and the numerical P_{num} are used separately in the similarity analysis and are not combined.

8. Similarity Analysis of the Numerical Calculations for Air and the Other Fluids

The second application of the similarity model uses the numerically calculated power for the various fluids: Air, R245fa, SES36, and HFE7100.

The numerical power of the reference fluid (Air), $P_{ref,Air}$ (=$P_{num,Air}$) is used to calculate the corresponding similarity power $P_{sim,R}$ for the other fluid "R".

In this calculation, the same inlet and outlet pressures p_{in}, p_{out}, and the rotational speed n are used for Air and for the other fluid "R".

Calculation of the similarity power $P_{sim,R}$ from the $P_{ref,Air}$ consists of four steps:

1. Calculation of the pressure loss $\Delta p_{loss,Air}$ (21) for the reference fluid Air for the known reference power $P_{ref,Air}$:

$$\Delta p_{loss,Air} = \Delta p_{in,out} - \frac{P_{ref,Air}}{n \cdot \Delta V_{geom}} \tag{39}$$

2. Calculation of the similarity constant B (35) for the particular expander using the pressure loss $\Delta p_{loss,Air}$ (39) for the inlet air viscosity $\mu_{in,Air}$ and density $\rho_{in,Air}$ at p_{in}, T_{in}:

$$B = \frac{\Delta p_{loss,Air}}{\mu_{in,Air}^{\gamma} \cdot \rho_{in,Air}^{1-\gamma} \cdot \frac{\left(1-\Delta p_{loss,Air}/p_{in}\right)^{2-\gamma}}{1-\Delta p_{loss,Air}/(2 \cdot p_{in})} \cdot n^{2-\gamma}} \tag{40}$$

3. Calculation of the similarity pressure loss $\Delta p_{loss,R}$ for the other fluid "R" by solving (numerically) the similarity equation using the constant B (40), and for the other fluid's "R" viscosity $\mu_{in,R}$ and density $\rho_{in,R}$ at the inlet p_{in}, T_{in}:

$$\frac{\Delta p_{loss,R}}{\mu_{in,R}^{\gamma} \cdot \rho_{in,R}^{1-\gamma} \cdot \frac{\left(1-\Delta p_{loss,R}/p_{in}\right)^{2-\gamma}}{1-\Delta p_{loss,R}/(2 \cdot p_{in})} \cdot n^{2-\gamma}} = B \tag{41}$$

4. Calculation of the similarity power $P_{sim,R}$ (21) for the other fluid "R" using the pressure loss $\Delta p_{loss,R}$ (41):

$$P_{sim,R} = n \cdot \Delta V_{geom} \cdot \left(\Delta p_{in,out} - \Delta p_{loss,R}\right) \tag{42}$$

The obtained similarity power $P_{sim,R}$ is further compared with the corresponding numerically calculated $P_{num,R}$.

The exponent parameter γ is determined for the particular pairs of Air and "R" by minimization of the sum of squares ϕ for the rotational speed n = 1500 and 3000 rpm:

$$\varphi(\gamma) = \sum_{n\,=\,1500,3000} \left[\left(P_{sim,R} - P_{num,R}\right)/P_{num,R}\right]^2 \tag{43}$$

The Golden Section method of minimization of ϕ gives the individual values of γ for the pairs of Air and R245fa, SES36, and HFE100 (Table 8).

Table 8. Exponent parameter γ for individual pairs of fluids and the common value.

γ, –	**Air, HFE7100**	**Air, SES36**	**Air, R245fa**	γ_{common}
	0.5861	0.6578	0.5733	0.6029

The minimization of ϕ for all the analyzed fluids gives the common value γ_{common}:

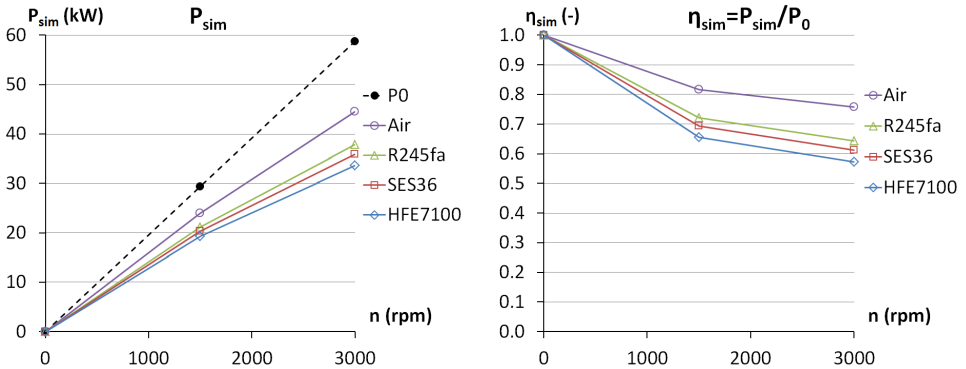
$$\varphi(\gamma_{common}) = \sum_{R = R245fa,\ SES36,\ HFE7100} \sum_{n = 1500,3000} [(P_{sim,R} - P_{num,R})/P_{num,R}]^2 \quad (44)$$

The common value γ_{common} (Table 8) is more correct in the sense of similarity, but the individual values of γ give slightly better agreement between the similarity power $P_{sim,R}$ and the corresponding numerical one $P_{num,R}$.

The similarity power $P_{sim,R}$ and the efficiency $\eta_{sim,R} = P_{sim,R}/P_0$ for the individual γ are presented in Table 9 and Figure 10. The values of $P_{sim,Air}$ and $P_{num,Air}$ (Table 7) are obviously equal.

Table 9. Similarity power $P_{sim,R}$ and efficiency $\eta_{sim,R} = P_{sim,R}/P_0$ for p_{in} = 16 bar(a) and p_{out} = 1 bar(a). The individual values of γ are used.

n rpm	P_{sim}, kW					$\eta_{sim} = P_{sim}/P_0$, –			
	HFE7100	**SES36**	**R245fa**	**Air**	**P_0**	**HFE7100**	**SES36**	**R245fa**	**Air**
0	0.000	0.000	0.000	0.000	0.000	1.0000	1.0000	1.0000	1.0000
1500	19.259	20.348	21.164	24.000	29.373	0.6557	0.6928	0.7205	0.8171
3000	33.582	35.936	37.831	44.550	58.745	0.5717	0.6117	0.6440	0.7584



(**a**) (**b**)

Figure 10. (**a**) Similarity power $P_{sim,R}$ vs. the rotational speed n for various working fluids and (**b**) efficiency $\eta_{\mathrm{sim,R}} = P_{sim,R}/P_0$. The dashed line shows the limiting power P_0 of the no-viscosity fluid.

The similarity power $P_{sim,R}$ for the various fluids, obtained from the reference numerical power $P_{ref,Air}$, is compared with the corresponding numerical power $P_{num,R}$ for the same fluids. Table 10 and Figure 11 present the ratio $P_{sim,R}/P_{num,R}$ for these fluids.

Table 10. Ratio P_{sim}/P_{num} vs. the rotational speed n for the various fluids.

n rpm	P_{sim}/P_{num}, –			
	HFE7100	**SES36**	**R245fa**	**Air**
0	1.0000	1.0000	1.0000	1.0000
1500	0.9508	0.9624	0.9662	1.0000
3000	1.0372	1.0283	1.0255	1.0000

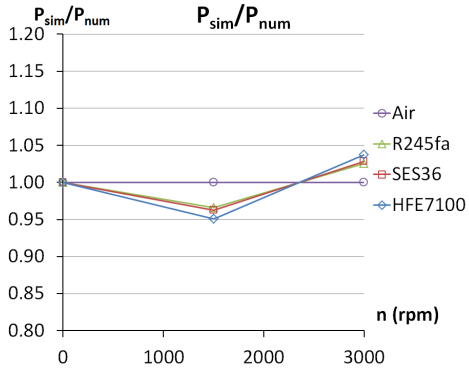


Figure 11. Ratio of the similarity $P_{sim,R}$ and the numerical power $P_{num,R}$ vs. the rotational speed n for the various fluids for the comparison of $P_{sim,R}$ and $P_{num,R}$.

The ratio $P_{sim,R}/P_{num,R}$ is calculated to compare $P_{sim,R}$ and $P_{num,R}$ and to present the relative errors of the approximation of $P_{num,R}$ by $P_{sim,R}$ in the analyzed ranges of pressure and rotational speed. The maximum relative error of P_{sim} vs. P_{mnf} is about ±5% (Table 9 and Figure 11), which is a rather good agreement. The same ±5% as in Section 6 is probably coincidental.

9. Discussion

The similarity model of the power P of a rotary lobe expander (Roots expander) is derived. It is based on the limiting power of no viscosity and on the similarity of the pressure losses. In this expander type, the volume transferred by the rotors from the inlet to the outlet is the same (the built-in volume ratio is equal to 1). The presented model concerns the similarity of pressure losses due to fluid viscosity, which decreases the power calculated for the ideal case of no viscosity. In this model, it is necessary to know the total volume transferred by the rotors within one shaft's revolution. The model was tested on the expander GGP16XA from Armak Motors, which was disassembled and measured.

The derived similarity model is rather simple. The intention was to develop an analytical, fast engineering tool for calculating the expander's power with acceptable accuracy as the more precise numerical calculation is expensive. In this model, the heat exchange with the ambient is not taken into account, along with the leakages. Two rotors are modeled by the single piston and the expander's geometry is represented by the volume ΔV_{geom} transferred by the rotors during the rotor shaft's revolution. Pressure losses are modeled by the single pressure loss at the high-pressure side, between the inlet and the piston.

The similarity model was tested both for the manufacturer's experimental power for Air and for the numerically calculated power for Air, R245fa, SES36, and HFE100. Additionally, the simple thermodynamic analysis for these fluids is presented. It shows the difference among these fluids in the generated power in the limiting case of no viscosity.

In the first application of the model, the manufacturer's values of power P_{mnf} (for five different inlet pressures and the rotational speed n = 0...3000 rpm) are approximated by the corresponding similarity power P_{sim}. The maximum relative error of this approximation is ±5%.

In the second application, the numerically calculated power from air $P_{num,Air}$ for p_{in} = 16 bar(a) and the rotational speeds n = 1500 and 3000 rpm is used to calculate the corresponding similarity power P_{sim} for the fluids R245fa, SES36, and HFE7100. The similarity power is compared with the numerically calculated power P_{num} for these fluids. The maximum relative error is again ±5%, which is probably a coincidence.

The presented simple similarity model may be useful for quickly calculating the expander's power for various fluids, pressure conditions, and rotational speeds with acceptable accuracy.

10. Conclusions

- The similarity model of the power of a rotary lobe expander (Roots expander) is derived. It is based on the limiting power of no-viscosity and on the similarity of the pressure losses.
- The novelty is the simple similarity model of this expander type, which may be used in the analytical and fast engineering calculation of the power before the more precise but expensive numerical calculation. It was tested in two applications.
- The first application is the approximation of the manufacturer's experimental power using the similarity power. The maximum relative error is $\pm 5\%$.
- The second application is the calculation of the similarity power for the fluids R245fa, SES36, and HFE7100 based on the numerical power for Air. The obtained similarity power is compared with the numerical powers for these fluids. The maximum relative error is again $\pm 5\%$ (it is potentially a coincidence).

Author Contributions: Conceptualization, W.R.; methodology, W.R.; software, W.R.; validation, W.R., A.M., Z.K. and S.B.; formal analysis, W.R., A.M. and Z.K.; investigation, W.R., A.M. and Z.K.; resources, S.B.; data curation, W.R.; writing—original draft preparation, W.R.; writing—review and editing, W.R.; visualization, W.R., A.M. and Z.K.; supervision, W.R.; project administration, S.B.; funding acquisition, S.B. All authors have read and agreed to the published version of the manuscript.

Funding: This research was partially supported by the National Centre for Research and Development in Poland (NCBiR) under project no. BIOSTRATEG 3/344128/12/NCBR/2017.

Institutional Review Board Statement: Not applicable.

Informed Consent Statement: Not applicable.

Data Availability Statement: The data presented in this study are available on request from the corresponding author due to the large volume of the results dataset.

Acknowledgments: The authors would like to thank Jarosław Mikielewicz from The Institute of Fluid-Flow Machinery for the fruitful discussions; e-mail: jaroslaw.mikielewicz@imp.gda.pl; address: IMP PAN, ul. Fiszera 14, 80-231 Gdańsk, Poland.

Conflicts of Interest: The authors declare no conflicts of interest.

Nomenclature

A	coefficient in the pressure drop equation, –
B	constant in the similarity equation, units are explained in Section 5
Eu	Euler number, –
h	specific enthalpy, J/kg
$\dot{m}$	mass flow rate, kg/s
n	rotational speed, 1/s
P	power, W
p	pressure (absolute), Pa
Re	Reynolds number, –
S	uncertainty
s	specific entropy, J/kgK
T	temperature, K
$\dot{V}$	volumetric flow rate, m^3/s
$\dot{V}_{geom}$	volumetric flow rate transferred by the rotors, m^3/s

v	fluid velocity, m/s
W	work produced during one shaft's revolution, J
Greek symbols	
γ	exponent in the pressure drop equation, –
ΔV_{geom}	volume transferred by the rotors during one shaft's revolution, m^3
η	efficiency, –
μ	dynamic viscosity, kg/ms
ρ	density, kg/m^3
φ	minimized objective function, –
Subscripts	
0	limiting case of no viscosity
geom	geometric (transferred by the rotors)
in	inlet
loss	losses (of the pressure)
m	mean value between the inlet and the piston
out	outlet
pst	near the piston
R	general name of the fluid
s	isentropic
mnf	manufacturer's experimental data
num	numerical calculation
sim	similarity calculation

Appendix A. Derivation of the Volume Transferred by the Rotors

The volume ΔV_{geom} transferred by the rotors in one shaft's revolution is a basic parameter in the presented similarity analysis. In the analyzed expander type, this volume does not change along the rotor's rotation, i.e., it remains the same from the inlet to the outlet.

For the particular analyzed expander, the volume ΔV_{geom} is derived analytically using the measured sizes of the disassembled expander, schematically shown in Figures 1 and 2.

The cross-sectional geometries of the upper and the lower rotors are shown in Figure A1. The volumes transferred by the upper and the lower gas pockets in 1/2 of one shaft's revolution (i.e., of the upper rotor) are shown in grey. The measured radii are r_1 = 36 mm, r_2 = 90 mm, r_3 = 29 mm, and r_4 = 63 mm. The length of both rotors is L = 100 mm. The distance between the rotors' axes is $r_1 + r_2$ = 36 mm + 90 mm = 126 mm. The ratio of the rotational speed of the lower n_l and the upper rotor n_u, connected by the gear train, is $n_l/n_u = r_1/r_2$ = 36 mm/90 mm = 2/5.

Analytical derivation of the volumes transferred by the upper and the lower rotor:

Because of the symmetry, only the values for $x \geq 0$ are used in the calculation.

In Figure A1a, the upper halves of three circles are given by the following equations:

$$y = \sqrt{r_1^2 - x^2} \ldots\ldots y = \sqrt{r_3^2 - (x - r_1)^2} \ldots\ldots y = \sqrt{r_4^2 - x^2} \quad \text{(A1)}$$

The coordinates of points A and B are determined from the systems of equations:

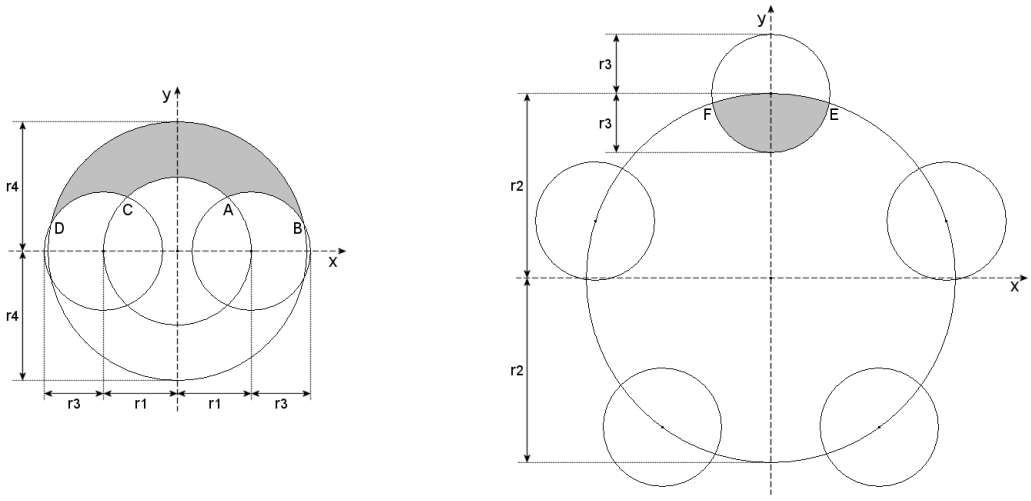
$$\begin{cases} y_A = \sqrt{r_1^2 - x_A^2} \\ y_A = \sqrt{r_3^2 - (x_A - r_1)^2} \end{cases} \ldots\ldots \begin{cases} y_B = \sqrt{r_4^2 - x_B^2} \\ y_B = \sqrt{r_3^2 - (x_B - r_1)^2} \end{cases} \quad \text{(A2)}$$

which gives the following:

$$x_A = \frac{2 \cdot r_1^2 - r_3^2}{2 \cdot r_1} = r_1 - \frac{r_3^2}{2 \cdot r_1} \ldots\ldots x_B = \frac{r_1^2 + r_4^2 - r_3^2}{2 \cdot r_1} = \frac{r_1}{2} + \frac{r_4^2 - r_3^2}{2 \cdot r_1} \quad \text{(A3)}$$

In Figure A1b, the upper and the lower halves of two circles are given by the following:

$$y = \sqrt{r_2^2 - x^2} \ldots\ldots y = r_2 - \sqrt{r_3^2 - x^2} \tag{A4}$$



(**a**) (**b**)

Figure A1. Geometry of the (**a**) upper rotor and the (**b**) lower rotor. The gas pockets, shown in grey, are transferred in 1/2 of the upper rotor's shaft revolution.

The coordinates of point E are determined from the system of equations below:

$$\begin{cases} y_E = \sqrt{r_2^2 - x_E^2} \\ y_E = r_2 - \sqrt{r_3^2 - x_E^2} \end{cases} \tag{A5}$$

which gives the following:

$$x_E = r_3 \cdot \sqrt{1 - \left(\frac{r_3}{2 \cdot r_2}\right)^2} \tag{A6}$$

The solutions are equal to the following:

$$x_A = 24.3194 \text{ mm} \quad x_B = 61.4444 \text{ mm} \quad x_E = 28.6212 \text{ mm} \tag{A7}$$

The volumes of the upper and lower gas pockets (Figure A1, in grey) are given by the following equations:

$$V_{pocket,u} = 2 \cdot (I_A + I_B) \cdot L \quad V_{pocket,l} = 2 \cdot I_E \cdot L \tag{A8}$$

where the integrals I_A, I_B, and I_E are given by the equations:

$$I_A = \int_0^{x_A} \left(\sqrt{r_4^2 - x^2} - \sqrt{r_1^2 - x^2} \right) dx \tag{A9}$$

$$I_B = \int_{x_A}^{x_B} \left(\sqrt{r_4^2 - x^2} - \sqrt{r_3^2 - (x - r_1)^2} \right) dx \tag{A10}$$

$$I_E = \int_0^{x_E} \left(\sqrt{r_2^2 - x^2} - r_2 + \sqrt{r_3^2 - x^2} \right) dx \tag{A11}$$

The integrals are solved analytically as follows:

$$I_A = 1/2 \cdot \left[r_4^2 \cdot arcsin\left(\frac{x}{r_4}\right) + x \cdot \sqrt{r_4^2 - x^2} - r_1^2 \cdot arcsin\left(\frac{x}{r_1}\right) - x \cdot \sqrt{r_1^2 - x^2} \right] \Big|_0^{x_A} \quad \text{(A12)}$$

$$I_B = 1/2 \cdot \left[r_4^2 \cdot arcsin\left(\frac{x}{r_4}\right) + x \cdot \sqrt{r_4^2 - x^2} - r_3^2 \cdot arcsin\left(\frac{x - r_1}{r_3}\right) - (x - r_1) \cdot \sqrt{r_3^2 - (x - r_1)^2} \right] \Big|_{x_A}^{x_B} \quad \text{(A13)}$$

$$I_E = 1/2 \cdot \left[r_2^2 \cdot arcsin\left(\frac{x}{r_2}\right) + x \cdot \sqrt{r_2^2 - x^2} - 2 \cdot r_2 \cdot x + r_3^2 \cdot arcsin\left(\frac{x}{r_3}\right) + x \cdot \sqrt{r_3^2 - x^2} \right] \Big|_0^{x_E} \quad \text{(A14)}$$

The upper and lower volumes transferred in one shaft's revolution are given as follows:

$$\Delta V_{geom,u} = 2 \cdot V_{pocket,u} \quad \Delta V_{geom,l} = 2 \cdot V_{pocket,l} \quad \text{(A15)}$$

which gives the following:

$$\Delta V_{geom,u} = 5.3718 \cdot 10^{-4}\ \mathrm{m}^3 \quad \Delta V_{geom,l} = 2.4609 \cdot 10^{-4}\ \mathrm{m}^3 \quad \text{(A16)}$$

The total volume transferred by two rotors in one shaft's revolution is equal to the following:

$$\Delta V_{geom} = \Delta V_{geom,u} + \Delta V_{geom,l} = 7.8327 \cdot 10^{-4}\ \mathrm{m}^3 \quad \text{(A17)}$$

References

1. Zhang, X.; Xu, Y.; Xu, J.; Sheng, Y.; Zuo, Z.; Liu, J.; Chen, H.; Wang, Y.; Huang, Y. Study on the performance and optimization of a scroll expander driven by compressed air. *Appl. Energy* **2017**, *186*, 347–358. [CrossRef]
2. Kovacevic, A.; Rane, S. 3D CFD analysis of a twin screw expander. In Proceedings of the 8th International Conference on Compressors and their Systems, London, UK, 9–10 September 2013.
3. He, W.; Wang, J. Optimal selection of air expansion machine in Compressed Air Energy Storage: A review. *Renew. Sustain. Energy Rev.* **2018**, *87*, 77–95. [CrossRef]
4. Capata, R.; Pantano, F. Expander design procedures and selection criterion for small rated organic rankine cycle systems. *Energy Sci. Eng.* **2020**, *8*, 3380–3414. [CrossRef]
5. Kolasiński, P.; Pomorski, M.; Błasiak, P.; Rak, J. Use of Rolling Piston Expanders for Energy Regeneration in Natural Gas Pressure Reduction Stations-Selected Thermodynamic Issues. *Appl. Sci.* **2017**, *7*, 535. [CrossRef]
6. Guillaume, L. On the Design of Waste Heat Recovery Organic Rankine Cycle Systems for Engines of Long-Haul Trucks. Ph.D. Thesis, University of Liège, Liège, Belgium, 8 November 2017.
7. Kolasiński, P. Application of volumetric expanders in small vapour power plants used in distributed energy generation—Selected design and thermodynamic issues. *Energy Convers. Manag.* **2021**, *231*, 113859. [CrossRef]
8. Żywica, G.; Kaczmarczyk, T.; Ihnatowicz, E. Expanders for dispersed power generation: Maintenance and diagnostics problems. *Trans. Inst. Fluid-Flow Mach.* **2016**, *131*, 173–188.
9. Parthoens, A.; Dumont, O.; Guillaume, L.; Lemort, V. Experimental and numerical investigation of a Roots expander integrated into an ORC power system. In Proceedings of the 24th International Compressor Engineering Conference, Purdue, West Lafayette, IN, USA, 9–12 July 2018.
10. Dumont, O.; Talluri, L.; Fiaschi, D.; Manfrida, G.; Lemort, V. Comparison of a scroll, a screw, a roots, a piston expander and a Tesla turbine for small-scale organic Rankine cycle. In Proceedings of the 5th International Seminar on ORC Power Systems, Athens, Greece, 9–11 September 2019.
11. Krawczyk, P.; Kurkus-Gruszecka, M.; Mikołajczak, A.; Łapka, P.; Badyda, K. Computational fluid dynamic analysis and validation of the single stage low pressure rotary lobe compressed air expander. *Therm. Sci.* **2019**, *23* (Suppl. S4), 1133–1142. [CrossRef]
12. Kurkus-Gruszecka, M.; Krawczyk, P. Comparison of two single stage low-pressure rotary lobe expander geometries in terms of operation. *Energies* **2019**, *12*, 4512. [CrossRef]
13. Liu, X.; Lu, J. Unsteady flow Simulations in a three-lobe positive displacement blower. *Chin. J. Mech. Eng.* **2014**, *27*, 575–583. [CrossRef]
14. Mălăel, I.; Costea, F.; Drăghici, M. Flow evaluation of the lobe pump using numerical methods. In Proceedings of the 3rd International Conference on Applied Physics, System Science and Computers, Dubrovnik, Croatia, 26–28 September 2018. [CrossRef]
15. Sedov, L.I. *Similarity and Dimensional Methods in Mechanics*, 10th ed.; CRC Press: London, UK, 1993; pp. 40–46.
16. Kuneš, J. *Similarity and Modeling in Science and Engineering*; Springer: Berlin/Heidelberg, Germany, 2012; pp. 107–112.

17. Armak Motors Corporation. Armak Gas Pressure Motor GGP16XA as Generatordrive. *The PDF File "11.4 GGP16XA-dat-1638 e.pdf"*. Available online: http://www.armakmotor.de (accessed on 22 September 2023).
18. Taylor, J. *An introduction to Error Analysis. The Study of Uncertainties in Physical Measurements*, 2nd ed.; University Science Books: Sausalito, CA, USA, 1997; pp. 60–62.
19. Brandt, S. *Data Analysis: Statistical and Computational Methods for Scientists and Engineers*, 4th ed.; Springer: Berlin/Heidelberg, Germany, 2014; pp. 36–40.
20. White, F.M. *Fluid Mechanics*, 7th ed.; McGraw-Hill: New York, NY, USA, 2011; pp. 347–430.
21. Kays, W.M.; London, A.L. *Compact Heat Exchangers*, 3rd ed.; Krieger Publishing: Malabar, FI, USA, 1998; pp. 35–38.
22. Dahlquist, G.; Björck, A. *Numerical Methods in Scientific Computing*; SIAM: Philadelphia, PE, USA, 2008; pp. 471–478.

Disclaimer/Publisher's Note: The statements, opinions and data contained in all publications are solely those of the individual author(s) and contributor(s) and not of MDPI and/or the editor(s). MDPI and/or the editor(s) disclaim responsibility for any injury to people or property resulting from any ideas, methods, instructions or products referred to in the content.